Journal of Materials Chemistry C

ROYAL SOCIETY OF CHEMISTRY

REVIEW

View Article Online
View Journal | View Issue

Check for updates

Cite this: J. Mater. Chem. C, 2021, 9, 12509

Polymers and interfacial modifiers for durable perovskite solar cells: a review

Dennis (Mac) Jones,† Yu An, Juanita Hidalgo, Caria Evans, Jacob N. Vagott and Juan-Pablo Correa-Baena *

This review focuses on the advancements in stability of perovskite solar cells under stress from ambient moisture, high temperatures, and UV light exposure. Moisture stability has been improved by utilizing several polymeric encapsulation methods, moisture-resistant hole transport layers (HTLs), CF_4 plasma treatments, and perovskite grain crosslinking. Fluorinated encapsulation methods have proven especially successful, producing cells that maintained their PCE after 75 days at 50% RH and 5 mW cm^{-2} of UV radiation. Temperature destabilization has been hypothesized to occur as a result of perovskite phase transitions and the HTL dopant migration to the mesoporous TiO_2 surface. Temperature-sensitive perovskites have been stabilized by tuning the Goldschmidt tolerance factor and introducing thermally resistant HTLs embedded in a polymeric matrix with polycarbonate acting as an effective thermal insulating matrix. UV light instabilities have also been shown to occur due to the photocatalysis of TiO_2 and the TiO_2 perovskite interface. The introduction of a Sb_2S_3 buffer or CsBr clusters as interface modifiers can stabilize the interface of TiO_2 perovskite. Herein, we aim at highlighting the main processes that prevent perovskite degradation using polymers and interfacial modifiers.

Received 17th March 2021,
Accepted 25th August 2021

DOI: 10.1039/d1tc01243f

rsc.li/materials-c

Published on 26 2021. Downloaded on 17.07.24 21:29:47.

1. Introduction

The rapid advancement of perovskite solar cells (PSCs) in recent years has propelled them to the forefront of renewable energy research. Since 2009, the power conversion efficiencies (PCEs) of PSCs have gone from 3.8% to 25.5% and are poised for further gains in the near future.[1] PSCs offer several advantages over competing technologies including their ease of processability, low manufacturing cost, and realistic potential for commercialization.[2] Many studies on PSCs involve maximizing PCE without compromising industrial scalability. However, there is still work to be done to ensure the stability of these devices under actual outdoor conditions.[3] This review focuses on the recent advances in the production of stable PSCs in common outdoor conditions.

Perovskite materials have an ABX_3 crystal structure, where A and B are organic or inorganic cations such as methylammonium and lead, respectively. X is an anionic inorganic halide, usually iodine or bromine, that resides at the unit cell's edge centers.[4,5] The perovskite structure allows for multiple low-cost fabrication methods, high charge carrier mobilities, and a tunable band gap. However, 3D perovskites are susceptible to penetration by water molecules, which can contribute to degradation of the perovskite, especially if present in combination with other common environmental factors such as UV light and high temperatures. Efforts to combat the long-term stability issues inhibiting perovskite absorbers have focused on encapsulation, crystal structure manipulation, and changes to selective contact layers. While progress has been made, there remains a need to further improve stability issues to allow for a wide range of industrial use of PSCs.

Polymers have been shown to improve the long-term stability of PSCs through encapsulation of the underlying layers, and can be modified relatively easily through processes such as fluorination. In addition, polymers have shown great promise as additives that have allowed for greatly improved outdoor stability; fluorinated polymers have enhanced moisture and thermal stability when compared to other common passivation and stability-enhancing additives. Therefore, the optimization of polymeric additives allows for finetuning of material properties and increase stability within perovskite solar cells. Similarly, utilizing polymeric charge transport layers allows for the direct use of thermal and moisture resistant materials. These materials can be optically tuned and easily modified for further optimization. This work will give an overview on how polymers have been used to enhance perovskite solar cell stability considering three main causes of degradation: (i) moisture, (ii) temperature, and (iii) UV-light.

School of Materials Science and Engineering, Georgia Institute of Technology, Atlanta, Georgia, USA. E-mail: jpcorrea@gatech.edu
† This author is deceased.

Published on 26 2021. Downloaded on 17.07.24 21:29:47.

2. Moisture-induced degradation

Most PSCs retain only 10–50% of their efficiency after a year of outdoor use, and this trouble has been one of the main roadblocks hindering commercialization.[6] A great portion of the stability challenge can be attributed to moisture-induced degradation. When focusing on the atomic scale, perovskites can breakdown from humidity alone. Stability against humidity is thus required in PSCs.

$$CH_3NH_3PbI_3\ (S) \leftrightarrow PbI_2\ (S) + CH_3NH_3I\ (aq) \quad (1a)$$

$$CH_3NH_3I\ (aq) \leftrightarrow CH_3NH_2\ (aq) + HI\ (aq) \quad (1b)$$

$$4HI\ (aq) + O_2\ (g) \leftrightarrow 2I_2\ (s) + 2H_2O\ (l) \quad (1c)$$

$$2HI\ (aq) \leftrightarrow H_2\ (g) + I_2\ (s) \quad (1d)$$

The susceptibility to moisture stems from the perovskite's preference to form an aqueous phase. For example, methylammonium lead triiodide ($MAPbI_3$) is easily hydrolyzed to aqueous methylammonium iodide (MAI) and solid lead iodide according to reaction (1a).[7] This aqueous phase is acidic and leads to the formation of hydrogen iodide (HI), which can breakdown and further shift the equilibrium towards degradation. The breakdown of HI can proceed by means regulated by either oxygen or UV radiation. In the case of oxygen, HI is easily oxidized to form iodine and water. UV light initiates a photochemical reaction that facilitates the breakdown of HI to hydrogen gas and iodine. Both processes contribute to further breakdown of the overall perovskite by shifting the equilibrium of eqn (1a) and (1b) to the right. Water's role in perovskite degradation can thus be thought of as an initiating role, where breakdown is further observed in the presence of other environmental factors. The overall ease of the degradation process drives researchers to perform PSC processing methods in a nitrogen atmosphere glovebox, an environment free of ambient moisture and oxygen.

2.1 Polymeric encapsulation

Polymeric encapsulation is a method to enhance the PSC stability by preventing moisture degradation. Most methods for enhancing the stability focus on altering a component of the PSC such as the hole transport layer (HTL) or even the perovskite absorber itself. However, encapsulation methods involve adding a new layer to the cell with goals including efficiency boosting and ensuring device stability. Polymers are great candidates for encapsulation due to their potential for hydrophobicity, transparency, crosslinking, and low free volume. Another advantage of polymeric encapsulation is their potential for UV curing, which allows for a tightly crosslinked network resisting moisture penetration without the need to add potentially damaging chemistry to the PSC.[8] Challenges include developing a hydrophobic polymer with a balance between low free volume and good transparency, while maintaining UV light, temperature, and moisture stability of both the PSC, and the polymeric encapsulation layer itself. The best encapsulation methods avoid efficiency losses which can occur either during the fabrication process due to the inert atmosphere or during operation due to reactions between the perovskite material and off-gassing vapors from the encapsulating material of choice. These methods can be applied across a wide range of devices and even work on perovskite quantum dots.[9]

Han *et al.* fabricated an encapsulated $MAPbI_3$ PSC depicted in Fig. 1A and B by depositing a UV curable epoxy resin in a glovebox purged with nitrogen and free of moisture.[10] The epoxy

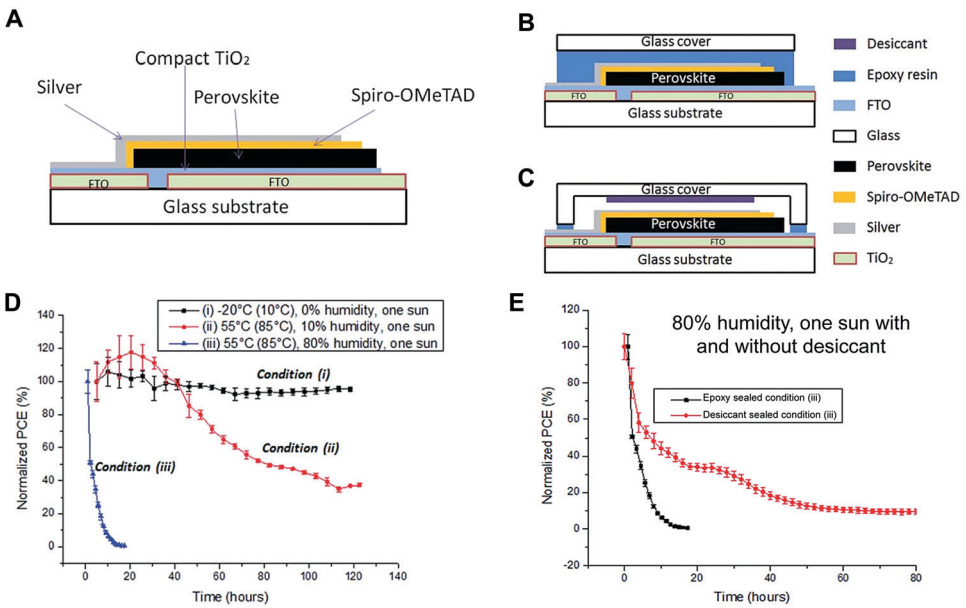

Fig. 1 Schematic cross-sections of unencapsulated (A), epoxy resin encapsulated (B), and epoxy/desiccant encapsulated (C) PSCs. Normalized PCEs of epoxy-only PSCs under three environmental conditions of increasing severity. Temperatures are reported as environmental temperature followed by the actual cell temperature in parenthesis (D). A comparison of PCE retainability between epoxy (black) and epoxy/desiccant (red) sealed PSCs under condition iii (E). Reproduced with permission from ref. 10. Copyright 2015 The Royal Society of Chemistry.

 This journal is © The Royal Society of Chemistry 2021

Published on 26 2021. Downloaded on 17.07.24 21:29:47.

encapsulation layer was fabricated on top of the fluorine doped tin oxide (FTO) layer and further topped with a glass cover. Two encapsulation methods were carried out. Fig. 1B depicts encapsulation with the epoxy resin alone and spanning the entire void between the FTO and glass cover. Fig. 1C depicts encapsulation using only enough epoxy resin to completely seal off the cell while adding a desiccant to absorb any moisture that may have penetrated through the thin epoxy layer during moisture stability testing. The desiccant is Dynanic's HG sheet, which can absorb water, but the degradation products of HI and methylammonium in the perovskite are not affected.[10]

A comparative analysis between the two methods can easily probe the epoxy resin's moisture sealing effectiveness. Stability testing results reported in Fig. 1D show a significant PCE drop of 60% at only 10% relative humidity (RH) after a slight initial increase.[10] The initial increase in PCE is not related to the penetration of moisture into the epoxy resin. Instead, PCE increases can be explained by annealing defects in the $MAPbI_3$ perovskite absorber. This annealing process is accelerated in the 85 °C cell temperature conditions, whereas defects remain in the perovskite layer with a cell temperature of only 10 °C. The PCE increase from the annealing process is quickly overpowered by perovskite hydrolysis at 40 hours for condition ii (annealing at 85 °C and humidity at 10%) and immediately for condition iii (annealing at 85 °C and humidity at 80%).

The 60 °C phase transition temperature of $MAPbI_3$ can explain most of the PCE loss in condition ii, but the vast difference in PCE retainment between conditions ii and iii suggests that $MAPbI_3$ perovskite is much more sensitive to moisture than temperature. This response supplements the argument that moisture is the most important environmental parameter to protect against. Not only is moisture the most damaging environmental effect to PCE, but it is also the parameter that sets off the entire hydrolysis degradation mechanism and is only exacerbated by other environmental factors.

The steep PCE loss observed in condition iii (Fig. 1D) as well as the disparity between PCE retainment in epoxy-only and epoxy/desiccant sealed cells (Fig. 1E) suggest that a significant amount of moisture is permeating through the epoxy resin. The desiccant delays complete PCE loss significantly, but the permeating moisture is either more than the desiccant can remove or bypassing the desiccant altogether. It should also be noted that the inclusion of the epoxy layer reduced efficiencies when compared to the unencapsulated device in Fig. 1A. This is likely a result of off-gassing compounds from the epoxy resin or a reduction in the doping of the 2,2′,7,7′-tetrakis[*N*,*N*-di(4-methoxyphenyl)amino]-9,9′-spirobifluorene (spiro-OMeTAD) HTL during the oxygen-free encapsulation process.[10] These results further promote the need to develop more stable and effective hydrophobic encapsulation layers for PSCs.

Other research into the field of polymeric encapsulation yielded similar results.[11–14] Matteocci *et al.* utilized a UV-curable glue and adhesive as a sealant for a PSC exposed to 30% RH for 170 hours.[12] The device retained 100% of its PCE throughout the test. In addition, Lee *et al.* found that depositing alternating layers of poly(1,3,5-trimethyl-1,3,5-trivinylcyclotrisiloxane) (pV3D3) and Al_2O_3 resulted in cells that retained 99.7% of their original 18.5% PCE over 300 hours at 50% RH.[11]

A popular solution to moisture permeability involves using fluorination to enhance the hydrophobicity of the encapsulation layer.[8,15–17] The interaction between water molecules and the surface is dominated by van der Waals forces, while electrostatic interactions are less. In order for the Van-der-Waals interaction to occur strongly on the surface, the molecules on the surface must be densely packed so that the water molecules can feel the combined van der Waals effect of adjacent surface molecules. Molecules containing C–F bonds are loosely packed, which causes water molecules to remain hydrogen-bonded instead of succumbing to the van der Waals attraction of the surface.[15] Fluorination is also desirable due to the stability and strength of the C–F bond, as well as their ability to repel both water and oil.

Bella *et al.* utilized a UV-curable fluoropolymer by spin-coating as an encapsulation layer for an organometal halide PSC as depicted in Fig. 2A.[8] Encapsulation methods included front side encapsulation, front/back side encapsulation, and unencapsulated PSCs for comparative purposes. Devices were subjected to 3 months in moisture-free UV illuminated air,

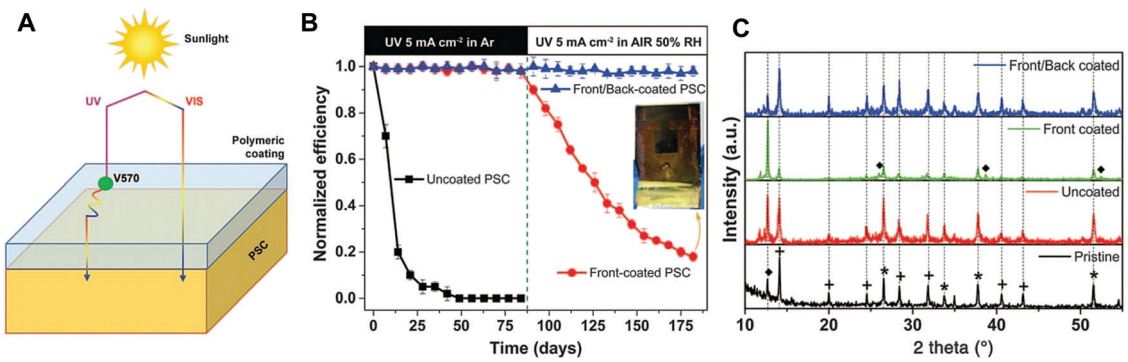

Fig. 2 Schematic illustrating the layout of a UV-curable fluoropolymer coated PSC (A). Normalized PCE as a function of time for front, front/back, and uncoated PSCs under 75 days of UV illumination followed by 75 days of UV illumination at 50% RH (B). Post-testing XRD patterns of the perovskite layers compared to a pristine perovskite sample. Peaks marked with a cross denote peaks attributed to the perovskite layer (C). Reproduced with permission from ref. 8. Copyright 2016 The American Association for the Advancement of Science.

Published on 26 2021. Downloaded on 17.07.24 21:29:47.

followed by 3 months is UV illuminated air at 50% RH. The front-coated devices gradually lost efficiency upon exposure to humid air due to the gradual influx of moisture into the devices' back sides leading to the hydrolysis of the perovskite layer, but front/back-coated devices retained their efficiency throughout the entire test (Fig. 2B).[8] The retained efficiency suggests that fluorination greatly decreased the amount of permeating moisture through the encapsulation layer when compared to UV-curable epoxy layers and highlighted the importance of sealing off the perovskite layer from all possible water access points. X-ray diffraction (XRD) patterns in Fig. 2C depict strong intensity losses in peaks associated with the perovskite layer for both uncoated and front coated devices, whereas front/back coated devices retained intensity in every perovskite related peak. Front and uncoated PSCs also showed PbI_2 peaks, which is a byproduct of perovskite hydrolysis as previously shown in eqn (1a).

Other fluoropolymers have been used in previous studies that have yielded similar results.[16–18] Griffini *et al.* demonstrated the use of a photocurable fluoropolymer encapsulation layer that withstood real world outdoor conditions for 2000 hours while maintaining its initial efficiency throughout the entire test.[16] In addition, Liu *et al.* utilized a hydrophobic organic fluoropolymer (HOFP) inserted between the active perovskite layer and the HTL to obtain stable PSCs that retained 80% of their initial efficiencies of 16.9% across a 2400 hour test in ambient conditions.[17] Multiple studies have since added to the success of fluorination in PSCs.[19,20]

Encapsulation methods are an effective way to combat the challenge of PSC stability, but they are far from the only practical method to approach this challenge. Changes can also be made to already existing layers of an unencapsulated PSC, such as the perovskite light harvesting layer. A simple and effective way to improve both stability and efficiency is to incorporate crystal crosslinking. Crystal cross-linking uses a cross-linking agent to tightly bond adjacent crystal grains of the perovskite light-collecting layer.[21,22] The crosslinking process smooths out the structure of the perovskite and allows for better charge carrier percolation throughout the cell. The smooth surface of a crosslinked perovskite crystal will therefore be more water-resistant. Crosslinking appears to block the extraction of MAI out of crosslinked $MAPbI_3$, which hinders the formation of lead iodide and stunts the perovskite hydrolysis.[21]

2.2 Attempts to form polymeric cations based on 2D perovskites

Remarkable efficiencies and large-scale production feasibility have made conventional 3D $MAPbI_3$ PSCs attractive candidates for commercialization. However, they are held back by challenges related to long-term stability and reproducibility issues.[23] Substituting the methylammonium (MA^+) cation with a bulkier cation such as a cationic polymer allows for perovskites to form in 2D with improved resistance to moisture and uniform morphology. 2D perovskites have a significant

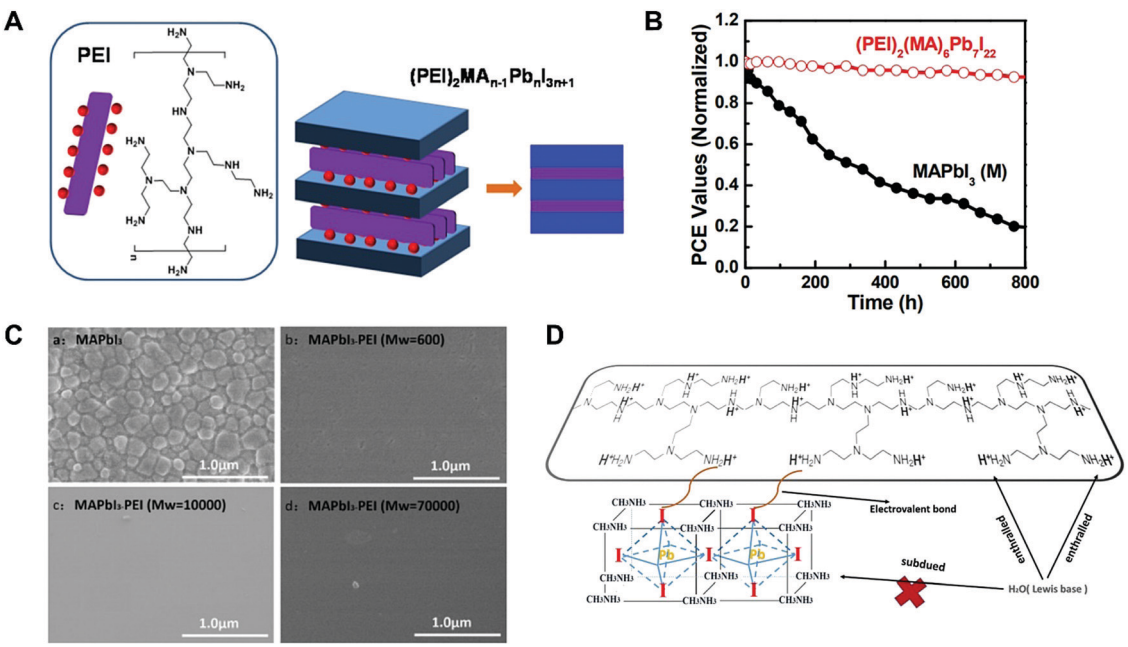

Fig. 3 The chemical structure of PEI cations used to produce 2D perovskite layers (A). The structure of the alternating 2D/3D perovskite layers that form when using a combination of methylammonium and PEI cations in the perovskite precursor solution. Stability of a 2D/3D layered PSC (red) and a conventional 3D methylammonium lead iodide PSC exposed to ambient humidity in the dark for 800 hours (B). Reproduced with permission from ref. 23. Copyright 2016 American Chemical Society. SEM images of control film $MAPbI_3$ and films with PEI (M_w = 600, 10 000 and 70 000) (C). An alternative proposed structure for PEI-modified perovskite layers (D). Reproduced with permission from ref. 24. Copyright 2018 John Wiley and Sons.

 This journal is © The Royal Society of Chemistry 2021

Published on 26 2021. Downloaded on 17.07.24 21:29:47.

stability advantage over 3D perovskites but suffer from decreased charge carrier mobilities and efficiency values.

Yao *et al.* studied the use of polyethyleneimine (PEI) cations in place of MA^+ with the goal of forming a multilayered perovskite alternating between 2D and 3D.[23] PEI was used to facilitate the formation of 2D perovskites and allowing for improved charge transport across 2D perovskite sheets when compared to conventional bulky ammonium cations. A schematic depicting the structure of the multi-layered perovskite is shown below in Fig. 3A.

Although the layered structure improves moisture resistance, the 2D layer acts as a barrier to charge extraction, thus reducing its efficiency. Increasing the molar ratio of PEI to MA^+ in the perovskite precursor solution will cause a sharp drop in PCE, but the stability will be significantly improved.[23] As shown in Fig. 3B, in the 800 hour test, the traditional 3D device lost 80% of its efficiency in the 800 hour test, while the stability test under the environment humidity without lighting can be stratified. PSC retained nearly 100% of PCE.[23]

A potential solution to retain stability improvements without giving up efficiency involves fabricating devices with only one 2D perovskite layer on the outer surface of the 3D perovskite, without allowing 2D perovskite layers to form in the bulk.

More recent research by Fairfield *et al.* discovered that the addition of polymers to the perovskite layer can reduce the size of the perovskite grains and prevent the formation of a hydrated phase that accelerates the degradation process.[25–27] This work showed similar results in terms of the stability of the added polymer but provided a different explanation for the decrease in initial efficiency. This work attributed the loss of efficiency to the smaller grain size and fewer pristine perovskite crystals associated with the polymer-coupled PSC.

Contrary to the Yao study[23] on the use of PEI, Wei *et al.* concluded that PEI could not replace MA^+ in the perovskite lattice to form 2D layers.[24] This was evidenced by efficiency losses upon the addition of PEI being attributed to an overall lower UV-vis adsorption spectrum rather than a band gap shift. Additionally, SEM images showed a grain size increase upon the addition of PEI rather than the decrease associated with previously mentioned studies using other polymers, Fig. 3C. This disparity suggests that PEI's amino and imine groups facilitated the growth of pristine perovskite films through their ability to be protonated. Protonated moieties can array at the grain boundaries through an ionic bond with iodine as shown in Fig. 3D.[24] This benefit allows for pristine growth whereas other polymers tend to avoid grain boundaries and interfere with crystal formation in the bulk. Nevertheless, PEI's reduction in UV-vis adsorption outweighs the grain size increase and produces an overall decrease in PCE from 9.69% to 6.84%. However, the PEI at the grain boundaries produces steric hindrance to protect perovskite grains from moisture, and similar encouraging stability results are seen when compared to the Yao study.

2.3 Moisture resistant polymeric HTLs and ETLs

The HTL incorporated into a PSC is often chosen with the goal of maximizing the efficiency of the device, but it is equally important to consider the role the HTL is playing in device stability. Hole transport materials (HTMs) often require hygroscopic dopants, which work against the goal of keeping ambient moisture out of the PSC to prevent perovskite hydrolysis.[28] Using spiro-OMeTAD as the HTM has produced efficient PSCs, but it suffers from low hole mobility, low conductivity in its pristine form, and poor stability when compared to competing HTMs.

Polymeric HTMs are good candidates to explore to overcome these challenges due to their tunable optical properties, low production costs, and potential to conduct holes without the need for incorporating hygroscopic dopants. Polymeric HTMs had previously been limited due to their poor penetration into mesoporous oxide films, leading to defect sites that resulted in undesirable charge recombination and efficiency losses. However, the development of extremely thin absorber layers allowed for better pore penetration and opened up the potential to research a variety of polymers as viable HTMs.[29]

Kwon *et al.* studied the use of poly[2,5-bis(2-decyldodecyl) pyrrolo[3,4-*c*]pyrrole-1,4(2*H*,5*H*)-dione-(*E*)-1,2-di(2,20-bithiophen-5-yl)ethene] (PDPPDBTE) and poly(3-hexylthiophene-2,5-diyl) (P3HT) as polymeric HTMs to replace spiro-OMeTAD (chemical structures shown in Fig. 4A).[30] When compared with spiro-OMeTAD, as shown in Fig. 4B, when tested on FTO substrates, both PDPPDBTE and P3HT show high water contact angles and it seems to provide their potential as stability-enhancing HTMs optimism. To test the stability, the PSCs were placed in an atmosphere maintained at 20% RH for 1000 hours without encapsulation.[31] The spiro-OMeTAD samples showed a 28% reduction relative to initial PCE, corresponding to a decrease in efficiency from 7.6% to 5.5% over 1000 hours (Fig. 4C). However, the PDPPDPTE and P3HT samples retained their initial efficiency values of 8.4% and 6.2% respectively. The stability improvements trace back to the HTM's hydrophobic nature outlined in Fig. 4B, which prevents water from accessing the perovskite absorber and causing its eventual hydrolysis.[30]

The work's boost in stability was especially encouraging when considering the thickness of the HTLs tested. The spiro-OMeTAD in the PSCs was 150 nm thick, whereas the polymeric HTLs were applied by spin coating at a much lower concentration, thus producing HTLs with a thickness of only 30 nm. The fact that polymeric HTLs can protect the perovskite absorber at such low thicknesses provides great optimism for future polymeric HTL research. This optimism is similar to that obtained from CF_4 plasma treatments, which protect the cell on length scales corresponding to the C–F bond.

Research has shown that the HTM hydrophobicity is strongly correlated to cell stability, but more testing is warranted to analyze the stability effects of dopants, especially in environments with humidity levels exceeding 20% RH. To be used industrially, more polymeric HTMs should be tested with and without dopants at humidity levels exceeding 20% RH to further separate polymeric HTMs from each other with regards to their stability effects.

Kim *et al.* studied the use of a dopant-free random copolymer (RCP) HTM shown in Fig. 4D based on benzo[1,2-*b*:4,5:*b*′]

Published on 26 2021. Downloaded on 17.07.24 21:29:47.

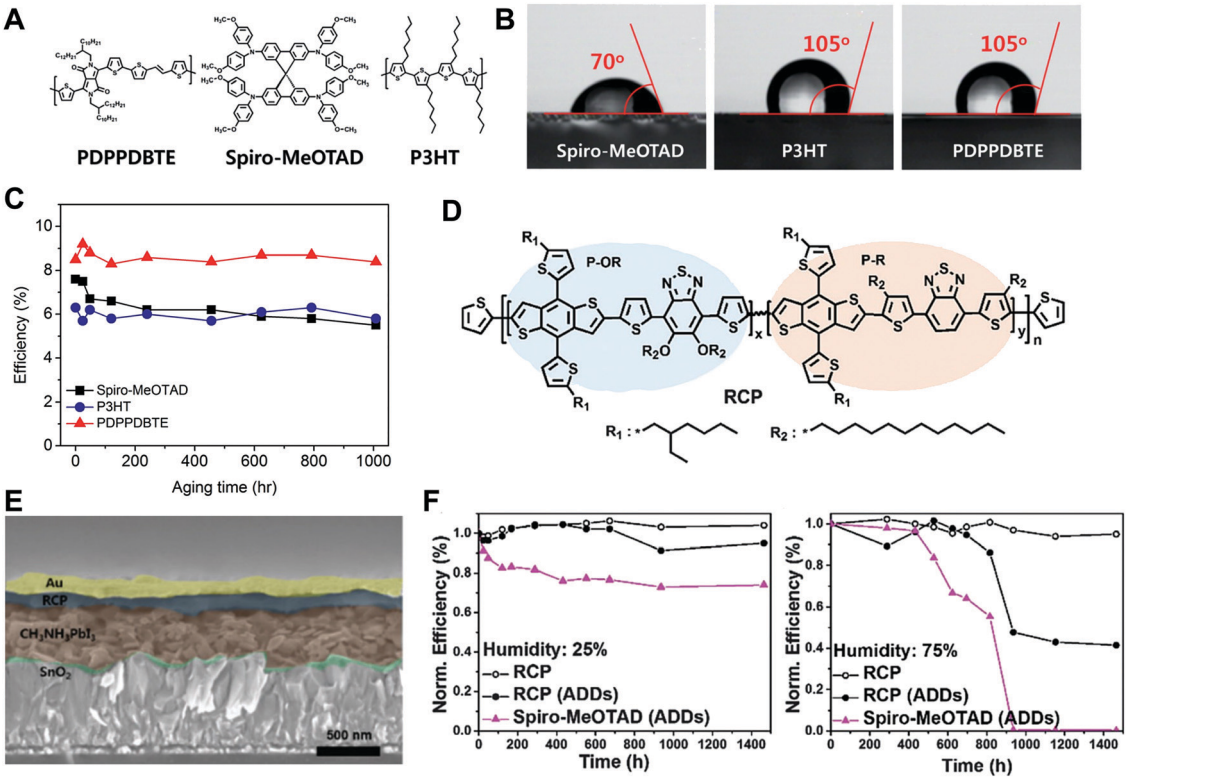

Fig. 4 Chemical structure of three common HTMs used in PSCs (A). Water contact angles associated with spiro-OMeTAD, P3HT, and PDPPDBTE HTLs (B). PCE stability associated with each HTL when used in unencapsulated PSCs at 20% RH (C). Reproduced with permission from ref. 30. Copyright 2014 The Royal Society of Chemistry. The chemical structure of the dopant-free RCP HTM. (D). A cross-sectional SEM image depicting the structure of the PSC. (E) Stability testing results of PSCs using the dopant-free RCP HTM, the doped RCP HTM, and doped spiro-OMeTAD at 25% RH. The initial efficiency was 17.3%. (F) The same stability results at 25% and 75% RH. Reproduced with permission from ref. 28. Copyright 2016 The Royal Society of Chemistry.

dithiophene (BDT) and 2,1,3-benzothiadiazole (BT).[28] The BDT moiety was chosen due to its efficient pi–pi stacking, which acts to increase charge transport and improve the HTM's hole mobility without the need to incorporate hygroscopic dopants that act to destabilize the perovskite absorber. The BT moiety was chosen to align the highest occupied molecular orbital (HOMO) energy level of the HTM to one slightly higher than the perovskite absorber, thus allowing for effective hole transfer from the perovskite absorber to the HTL. The organic moieties labeled R_1 and R_2 were incorporated with the goal of enhancing the HTL's hydrophobicity and thus the overall stability of the PSC. A solution of the RCP HTM was spin-coated atop the perovskite absorber to yield a thin polymeric HTL as depicted by the cross-sectional SEM image in Fig. 4E.[28]

Testing of the long-term stability of the PSCs was carried out by exposing the devices to humidity levels of 25% RH and 75% RH for 1400 hours without encapsulation. Two devices, one using the RCP HTM and the other using spiro-OMeTAD contained lithium bis(trifluoromethanesulfonyl)imide (LiTFSI) dopants. The third device used the RCP HTM without the presence of added dopants. The results in Fig. 4F show that not only are the presence of dopants ineffective to boost the RCP's hole mobility, but also that they diminish the stability of the cell. This stability decrease is due to the hygroscopic nature of LiTFSI. The LiTFSI attracted moisture from the humid environment and produced yellow lead iodide as a byproduct of the perovskite absorber's hydrolysis. At 25% RH, both RCP HTLs were able to retain cell efficiency. However, at 75% RH, the presence of LiTFSI in the RCP reduced the normalized PCE by 60%, yet still obtained better results than with the doped spiro-OMeTAD.[28] This result suggests that the RCP is providing two benefits to the cell: the first being its hydrophobicity and the second stemming from its lack of required hygroscopic dopants. The full effect of RCP stability enhancement is on display in the cell with an undoped RCP HTM, where normalized PCE is retained throughout the entire 1400 hour test at both 25% and 75% RH. Other researchers have obtained similar efficiency and stability boosting results from dopant-free HTMs.[31–35]

Bai *et al.* explored the use of branched fullerene chemistry as an electron transport layer (ETL).[36] Cyclic C_{60} fullerene formed a self-assembled monolayer (SAM) atop the perovskite layer. The stability of the SAM is attributed to hydrogen bonding between carboxylic acid groups attached to the fullerene. The SAM is then further modified by adding a silane coupling agent as shown in Fig. 5. This coupling agent bonds to the SAM *via* the exposed carboxylic acid moieties and allows for the formation of a siloxane chain across the ETL to effectively crosslink the entire layer. In addition, the coupling agent is terminated with carbon-fluorine bonds, which have already been discussed in Section 3.2 as being hydrophobic. These ETLs resulted in PSCs that retained

 This journal is © The Royal Society of Chemistry 2021

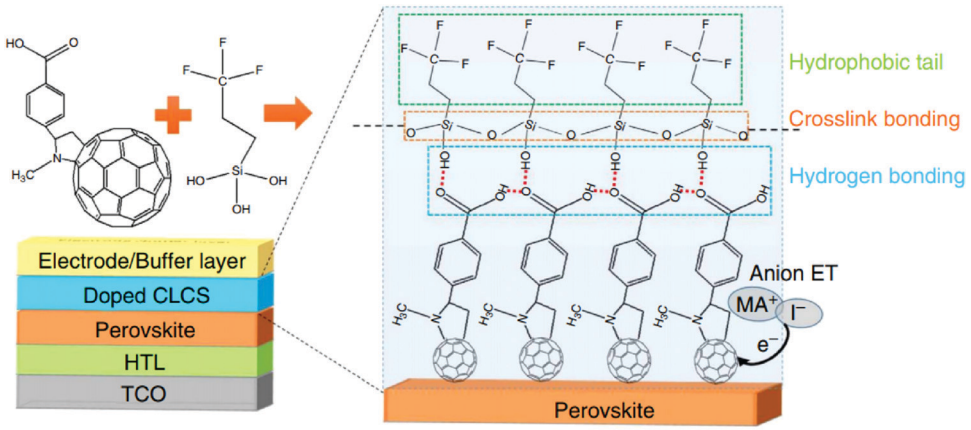

Fig. 5 A schematic depicting a doped fullerene ETL and the purpose of various moieties. Reproduced with permission from ref. 36. Copyright 2016 The Author(s), published open access by Springer Nature under the terms of the Creative Commons CC-BY license.

Published on 26 2021. Downloaded on 17.07.24 21:29:47.

90% of an initial PCE of 19.5% across a 30 day test in an ambient environment.[36] Further studies have concluded that fullerene chemistry can also conjugate with polymers such as PMMA to provide similar moisture resistance.[37]

Polymeric HTLs and ETLs require addressing several challenges, such as ensuring adsorption spectra that do not overlap with the perovskite absorber, allowing for strong pi–pi stacking and incorporating hydrophobic functional groups for enhanced stability. However, efficiency boosts resulting from their use prove favorable, and they further supplement the advantages of polymeric encapsulation methods and crystal crosslinking. In addition to their ease of processing, their ability to prevent perovskite hydrolysis at humidity levels of 75% RH makes them some of the most powerful tools to bolster PSC stability to date.

3. Temperature resistance

The increase of temperature is necessary for perovskite deposition processes, and some devices even show slight temporary efficiency increase with temperature as defects in the perovskite absorber layer anneal out. However, as phase transitions begin to occur, high temperatures pose a threat to the structure and stability of the perovskite. Temperature can even affect the stability and performance of other layers other than the perovskite layer, such as the HTL. This section analyzes the effect of temperature on the perovskite structure and HTL stability and discusses methods to maintain PSC stability under high temperature conditions.

$$\text{tolerance factor} = \frac{r_a + r_x}{2\sqrt{r_b + r_x}}$$

In order to maintain optimum light-harvesting properties, perovskite absorbers must remain in this structure.[39] The Goldschmidt tolerance factor involves a relationship between the atomic sizes of the perovskite crystal's atoms.[38] The perovskite structure is most stable when the Goldschmidt tolerance factor is between 0.8 and 1.[40–42] At tolerance factors above 1, a large A cation or small B cation causes the perovskite to become more stable in a hexagonal structure. At tolerance factors below 0.8, small A cations cause the perovskite to become more stable in an orthorhombic structure. Perovskites with the highest temperature stability resist temperature-induced phase changes by maintaining a tolerance factor between 0.8 and 1, where a significant increase in temperature is required to destabilize the perovskite structure. Atoms in perovskite structures are often changed for efficiency or environmental reasons, but it is important to pay close attention to the relative atomic sizes of the ions in use if temperature stability is desired. Fig. 6 describes a simple example of temperature's effects on PSC performance. Quarti *et al.* studied the effects of temperature on the efficiency of a $MAPbI_3$ PSC.[38] When heating from 300 K to 360 K, the normalized EQE is significantly reduced due to the tetragonal cubic phase transition and the subsequent increase in the band gap. However, cooling the device back to 300 K resulted in a complete reversibility to the more efficient tetragonal phase.[38]

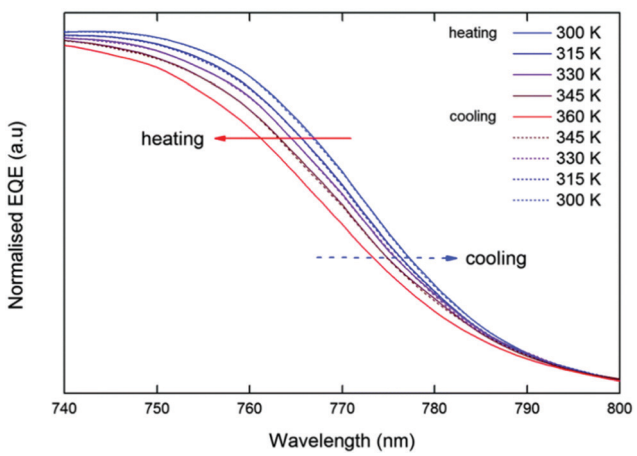

Fig. 6 Normalized external quantum efficiency (EQE) for a methylammonium lead iodide-based PSC at a temperature range spanning a tetragonal-cubic phase transition. Reproduced with permission from ref. 38. Copyright 2016 The Royal Society of Chemistry.

Published on 26 2021. Downloaded on 17.07.24 21:29:47.

Although the perovskite absorber is at the risk of phase transitions during temperature exposure, it is not the only PSC component of interest when considering temperature-related stability. The HTL's temperature stability should also be noted, as well as its effectiveness of protecting the perovskite absorber from temperature increases outside the cell. Conventional spiro-OMeTAD suffers from complications arising from increased temperatures during the annealing process such as dopant migration to the TiO_2/perovskite absorber interface.[43] Although annealing promoted HTM oxidation, thereby improving hole transport and cell efficiency, the increase in temperature caused the Li-TFSI dopant to migrate to the mesoporous TiO_2 surface and lower the Fermi level. This problem has led to research aiming to discover more temperature-stable HTMs with the ability to both perform at high temperatures and protect the PSC's overall stability.

Habisreutinger *et al.* studied the use of polymer-functionalized single-walled carbon nanotubes (SWNTs) insulated within a polymethyl methacrylate (PMMA) matrix as a thermally stable and thermally insulating HTL.[43] Fig. 7A depicts the structure of the proposed PSC containing P3HT/SWNT nanohybrid mesh surrounded by PMMA. Although PMMA provides excellent thermal stability and insulation, it lacks the pi–pi stacking necessary for effective hole transport to produce an efficient PSC on its own. For this reason, a P3HT/SWNT mesh is placed within the PMMA matrix to provide both effective hole transport and thermal stability.[43] The SWNTs also allow for a direct contact line between the perovskite absorber and the metal cathode to further enhance hole mobility. In addition to providing thermal stability, the presence of the PMMA matrix also acts to prevent efficiency losses arising from charge recombination at the HTL/perovskite interface.

The P3HT/SWNT HTLs insulated with PMMA were tested for temperature stability against controls using spiro-OMeTAD, P3HT, and PTAA HTLs without PMMA insulation. As shown in Fig. 7B, temperatures ranged from 25 °C to 100 °C, and PCE was measured after letting the unencapsulated PSCs equilibrate at

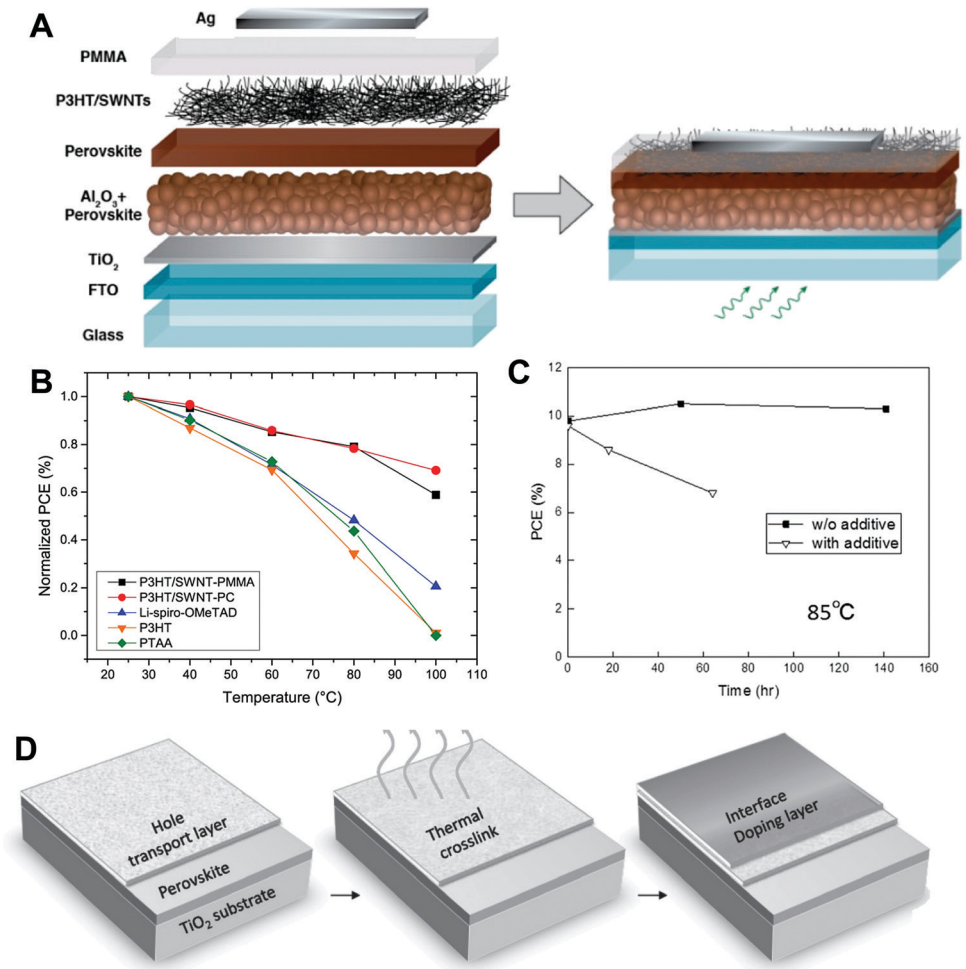

Fig. 7 Schematic illustrating the structure of a PSC with a P3HT functionalized SWNT HTL embedded within a PMMA matrix. The PSC utilized a mesoporous Al_2O_3 network on a glass substrate (A). Normalized PCE as a function of temperature and HTM type. Red and black curves represent embedded HTLs, while green blue and orange curves represent pristine HTLs (B). Reproduced with permission from ref. 43. Copyright 2014 American Chemical Society. PCE *vs.* time at 85 °C for a PSC using a poly(triarylamine) (PTAA) HTL with and without dopants (C). Reproduced with permission from ref. 44. Copyright 2016 John Wiley and Sons. The two-step process for forming a thermally crosslinked HTL (D). Reproduced with permission from ref.45 Copyright 2016 John Wiley and Sons.

 This journal is © The Royal Society of Chemistry 2021

Published on 26 2021. Downloaded on 17.07.24 21:29:47.

each temperature tested for 20 minutes.[43] This characterization technique is a particularly difficult test when considering that solar cells typically only experience temperatures reaching 85 °C in the hottest environments. The benefits of the PMMA insulation can immediately be seen, and lead to better PCE retainment when compared to unembedded HTLs. Polycarbonate (PC) was an especially effective thermal insulator at high temperatures, surpassing PMMA beyond temperatures of 80 °C to produce PSCs retaining 75% of their original PCE.

Matsui *et al.* found equally encouraging results when testing a dopant-free PTAA HTL at 85 °C.[44] However, dopants designed to increase charge transport decreased stability, as illustrated in Fig. 7C. It's theorized that dopants facilitate the diffusion of gold into the perovskite layer at high temperatures, thus reducing the crystal purity, V_{oc}, and fill factor of the cell. Nevertheless, multiple studies have shown the success of temperature-resistant HTLs.[46–49]

Xu *et al.* proposed thermal crosslinking to solve temperature stability issues and the process is shown in Fig. 7D. Crosslinked molecules are known to withstand higher temperatures than their linear counterparts.[45] Xu *et al.* started with *N*4,*N*4′-di(naphthalen-1-yl)-*N*4,*N*4′-bis(4-vinylphenyl)biphenyl-4,4′-diamine (VNBP), which contains two double bonds that can be used for polymerization. After the thermal crosslinking was carried out, a layer of MoO_3 was deposited atop the HTL to improve charge extraction. The device maintained 90% of its original efficiency of 16.5% after an hour of annealing at 110 °C and remained stable after 30 days at 70% RH. Control devices using spiro-OMeTAD HTLs broke down immediately after the 110 °C annealing step, and XRD tests showed PbI_2 peaks after only 10 days at 70% RH.[45] Although temperature damage to perovskite absorbers is reversible, the damage to the unembedded pristine HTLs remained after cooling, suggesting that the temperature instabilities of P3HT and PTAA are permanent.

The PMMA and PC matrix embedding also provided significant moisture resistance to the PSC. Water contact caused degradation into PbI_2 (yellowing) of the unembedded devices, whereas the embedded devices remained their original color. Unlike the PSCs with pristine HTLs, the PCE of the embedded devices was well retained, suggesting that water does not interfere with the ability of the SWNTs to conduct holes. Combining conventional encapsulation methods with polymer-functionalized SWNT HTLs should lead to thermally-resistant moisture-stable PSCs suitable for use on the industrial scale, especially when considering the low manufacturing costs of PC and PMMA.

4. UV light stability

In Section 2.1, UV light was shown to degrade the perovskite absorber indirectly by promoting the conversion of hydrogen iodide to hydrogen gas and iodide, thus shifting the equilibrium of the hydrolysis process towards degradation. However, UV light can also destabilize the perovskite absorber directly *via* a photocatalytic effect of TiO_2 at the mesoporous TiO_2 perovskite interface. Determining the mechanism of UV light degradation is challenging due to its participation in other more dominant degradation processes such as moisture-related instabilities. Consequently, UV light stability tests must be conducted in a glove box completely void of ambient moisture near room temperature.[50,51] This section aims to analyze the UV degradation mechanism at the perovskite/TiO_2 interface as well as explore effective interfacial modification methods to prevent perovskite degradation.

4.1 Antimony trisulfide interfacial modifiers

Ito *et al.* studied the degradation of a $MAPbI_3$ PSC exposed to UV light for 12 hours.[50] By the end of the exposure, the PSC had lost all its efficiency. The problem is presumed to result from instabilities at the TiO_2/perovskite interface. Fig. 8A depicts a schematic describing the breakdown of the perovskite layer *via*

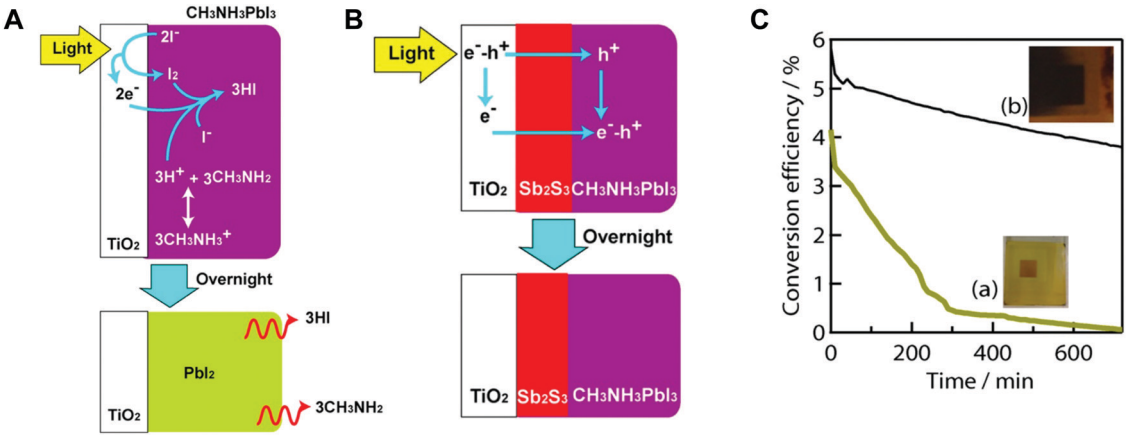

Fig. 8 A schematic illustrating the UV-induced degradation of $MAPbI_3$ at the TiO_2 interface (A). Protection against UV light degradation in a PSC containing an antimony trisulfide (Sb_2S_3) layer between the mesoporous TiO_2 and the perovskite absorber. PCE retainment of an unmodified and unencapsulated methylammonium lead iodide PSC (A) *vs.* an antimony trisulfide modified PSC (B) under UV light with an intensity of 100 mW cm^{-2} for 12 hours. Photographs of the device showing PbI_2 discoloration in the unmodified PSC are included (C). Reproduced with permission from ref. 50. Copyright 2014 American Chemical Society.

Published on 26 2021. Downloaded on 17.07.24 21:29:47.

UV light exposure. TiO_2 interacts with perovskite absorbers by withdrawing electron density away from the halogen, in this case an iodide anion.[50] This leads to the formation of I_2, leaving MA^+ behind. Without the exposure to UV light, this process is in an equilibrium dominated by the perovskite structure. However, continuous UV light exposure facilitates the loss of MA^+ and HI, which drives the equilibrium toward the PbI_2 degradation product and turns the PSC a yellow color at the TiO_2/perovskite interface.

Fig. 8B depicts an efficient method to combat perovskite degradation from UV light exposure. A thin layer of Sb_2S_3 is deposited between the mesoporous TiO_2 and the perovskite absorber to stop perovskite degradation at its source.[50] The Sb_2S_3 layer acts as a buffer between the compact TiO_2 and perovskite layers and prevents TiO_2 from extracting electron density from the iodide anion which in turn hinders the formation of I_2. The inhibition of I_2 formation is vital, since it kicks off the entire UV light degradation process. However, the Sb_2S_3 layer continues to allow charge transport to and from the mesoporous TiO_2 and the perovskite absorber. The PSC is therefore rendered immune to UV light degradation while maintaining its previous efficiency.[50]

The stability improvement was confirmed by exposing the PSC to UV light (100 mW cm^{-2}) for 12 hours in a glove box at 0% RH. Fig. 8C confirms that within just 4 hours, the efficiency of the control PSC fell to less than 1%, while the PSC containing an antimony trisulfide interlayer between the mesoporous TiO_2 and the perovskite maintained better stability.[50] Photographs of the solar cell confirmed a yellowing of the unmodified PSC due to PbI_2 formation, which further suggests significant perovskite degradation *via* UV light. Although the interlayer hinders degradation, the PCE drop-off is still apparent in modified devices. The remaining stability issues warrant further modification studies regarding the TiO_2/perovskite interface.

4.2 Cesium bromide interfacial modifiers

Li *et al.* explored yet another approach to combat the issue of TiO_2 photocatalysis by coating a layer of CsBr atop the compact TiO_2 as shown in Fig. 9A and B.[52] The stability was tested without encapsulation, and results were obtained after exposing the PSCs to 365 nm UV light equating to 113 suns.[52] Samples were tested over 50 minutes of continuous exposure in dry air. Unlike the previous example of Sb_2S_3, the CsBr layer formed discontinuous clusters as opposed to a continuous thin film (Fig. 9B). It is therefore difficult to argue that a stability enhancing mechanism results from the CsBr interlayer shielding the contact between the compact TiO_2 and the perovskite completely. However, it is theorized that the cesium ions prevent TiO_2 from achieving full photocatalysis at its active sites, thus preventing the formation of a yellow PbI_2 layer at the TiO_2/perovskite interface.

The deactivated photocatalytic TiO_2 sites resulted in PSCs that retained 70% of their initial efficiency after 20 minutes of testing, whereas the control samples lost all their efficiency during the same time period, as illustrated in Fig. 9C. However, further exposure resulted in continued yet slowed perovskite degradation. In addition to reduced TiO_2 reactivity, the efficiency boost is thought to be attributed to a reduced defect concentration at the TiO_2/perovskite interface in the presence of CsBr. These defect sites are most likely points of degradation onset. Both defect concentration and TiO_2 reactivity should be accounted for in further studies aimed at the inhibition of UV-induced perovskite degradation.[52]

4.3 Polymeric HTLs to enhance PSC photostability

Tsai *et al.* tackled the issue of photostability by focusing on the HTL.[54] They realized that conventional HTLs like PEDOT:PSS (chemical structure shown in Fig. 10A) packed well and produced good hole mobility but failed to block or absorb light

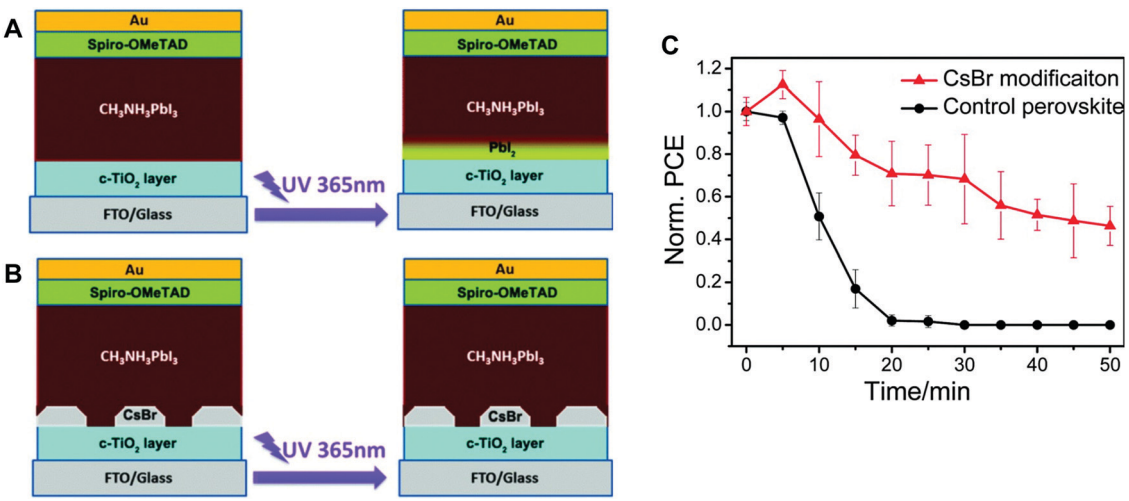

Fig. 9 Schematic depicting a PSC containing a typical compact TiO_2/perovskite interface before and after UV exposure (A). A PSC containing cesium bromide (CsBr) interfacial modifiers before and after UV exposure (B). Normalized PCE for CsBr modified (initial PCE of 15.3%) and control (initial PCE of 11.3%) devices as a function of time under 100 mW cm^{-2} UV light (C). Reproduced with permission from ref. 52. Copyright 2016 The Royal Society of Chemistry.

 This journal is © The Royal Society of Chemistry 2021

Published on 26 2021. Downloaded on 17.07.24 21:29:47.

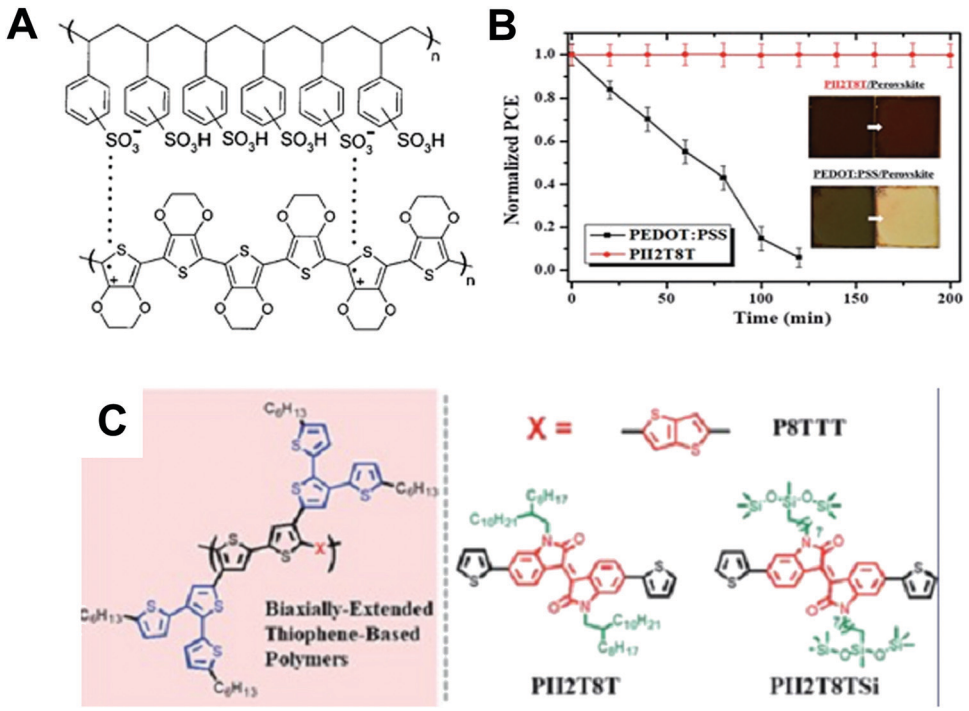

Fig. 10 Chemical structure of poly(3,4-ethylenedioxythiophene):poly(4-styrenesulfonate) (PEDOT:PSS) (A). Reproduced with permission from ref. 53. Copyright 2008 Elsevier. Normalized PCE of a PSC utilizing PEDOT:PSS (black) and PII2T8T HTLs under a 365 nm UV lamp (5 mW cm^{-2}) and 50% RH (B). The chemical structure of various tested HTLs. The moiety "X" is either P8TTT, PII2T8T, or PII2T8TSi (C). Reproduced with permission from ref. 54. Copyright 2018 The Royal Society of Chemistry.

in the UV spectrum. To solve this issue, polymers with bulky side chains were sought out with the aim of using these groups to take in UV radiation. P8TTT (Fig. 10C) has achieved success in this regard. However, the researchers pointed out that due to the steric hindrance of the side groups and the poorly filled backbone, there is a decrease in hole mobility. To combat this issue without giving up UV adsorption, electron withdrawing moieties were added to the backbone in place of the P8TTT.

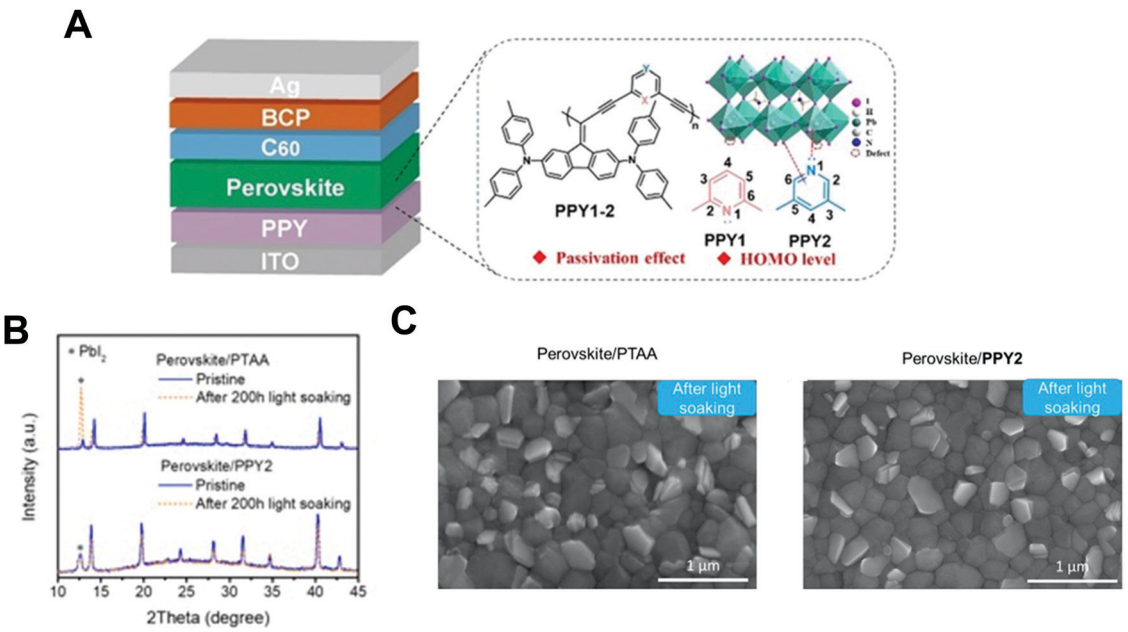

Fig. 11 Schematic of device and potential interfacial interaction between perovskite layer and PPY-based HTL (A). XRD patterns of PTAA control/perovskite films and PPY-2/perovskite films before and after 200 h light soaking (B). SEM images of perovskite/PTAA films and PPY-2/perovskite films after light soaking (C). Reproduced with permission from ref. 61. Copyright 2021 John Wiley and Sons.

Published on 26 2021. Downloaded on 17.07.24 21:29:47.

These were PII2T8T and PII2TiTSi; two similar moieties bringing superior hole mobility to the HTL. The PII2T8T modified HTL maintained a PCE of 18.32% under 5 mW cm^{-2} of UV light at 50% RH for 200 minutes while the devices using PEDOT:PSS immediately decayed from their initial PCE of 16.40%.[54] More studies have utilized polymeric HTLs or ETLs to stabilize PSCs against UV degradation with similar results.[55–60]

Dopant-free HTLs have also been explored for the enhanced photostability of PSCs. Sun *et al.* reported the use of a dopant-free pyridine-based HTL to reduce non-radiative recombination and improve photostability and efficiency.[61] Pyridine is a widely used Lewis base for the passivation of undercoordinated lead at the perovskite surface and an ideal electron-acceptor unit of donor–acceptor HTL. In efforts to reduce defects on the perovskite surface and correct HTL band misalignment, Sun employed the use of a pyridine monomer for the HTL.[61] As shown in Fig. 11A, the structure of PPY1–2 is distinguishable by the linkage positions of pyridine unit, PPY-1 having the link in the X position and PPY-2 in the Y position.[61] The pyridine unit at the different positions resulted in a HOMO level regulation, with PPY-2 exhibiting better matched HOMO levels to the perovskite. PPY-2 also had higher mobilities and better exposure for passivation of defects.[61] SEM and XRD measurements were used to examine photostability of the perovskite with the PPY-2 and commonly used HTL, PTAA (Fig. 11B and C).[61] Fig. 11B shows the XRD patterns of the light-soaked films, after 200 h, the PTAA/perovskite film exhibited a significant increase of the PbI_2 signal located at 12.5° indicating degradation; however, the PPY-2/perovskite film remained relatively unchanged. SEM images supported this finding as the PTAA/perovskite film had denser PbI_2 particles, which suggests degradation, Fig. 11C. The morphology of the PPY-2/perovskite did not result in any noticeable changes.[61] The increase of photostability of PSCs is attributed to the surface passivation effect seen more prominently in PPY-2. PPY2-based devices maintained over 97% of initial PCE after 500 h, with almost no decline in all device parameters, while the PTAA control devices retained only 75% of the initial PCE.[61] Dopants employed in commonly used HTMs have proven to be detrimental to the stability of PSCs; more studies have explored the development and use of dopant-free HTMs for more stable and efficient PSCs.[62]

5. Conclusion

Reproducible and reliable PSC long-term stabilities have proven difficult to obtain upon exposure to moisture, high temperatures, and UV light. However, advancements in polymers and interfacial modifiers have successfully produced stable PSCs under each of the three environmental conditions. Despite encouraging results, more work is needed to pay attention to the stability of PSC while considering the environmental impact. This area of study will accurately represent what PSCs will experience outside the lab and allow for faster implementation of industrial scale PSC development. Studying PSC stability under various environmental influences may lead to the use of a combination of stabilization techniques to test devices. Studies involving these combinations are important, as they have the potential to ensure the effective use of multiple stabilization techniques without negative consequences arising from interference between each technique. For example, they could ensure effective contacts between encapsulation layers and modified HTLs, or incorporate crystal crosslinking in the presence of interfacial modifiers at the TiO_2/perovskite interface.

Polymers could be widely applied in the perovskite layer as additives to regulates the crystallization of perovskite films and can also be used as interfacial modifiers to enhance the performance and stability of PSC. Furthermore, polymers can be employed as HTL, ETL, and encapsulation materials to improve the durability of PSC under stress from ambient moisture, high temperatures, and UV light exposure. Particularly, polymer HTLs have been studied extensively due to their versatile and adjustable chemical and physical properties. Dopant-free polymer HTLs have experienced rapid development in the past few years and have unambiguously demonstrated superior moisture stability, benefiting from the removal of the hygroscopic dopant. Unfortunately, there is still room for improvement in device efficiency when compared to top-performing doped polymers. In this regard, the design of efficient dopant-free polymer HTL with appropriate energy level alignment to enhance charge mobility is urgently needed to boost the efficiencies of PSC. The development of cross-linkable polymer HTL will also be worthy of consideration in the future since the three-dimensional network structures of polymers provide a higher density of the charge-transport channels, a superior solvent/thermal resistance, and mechanical durability, which are conducive to the fabrication of inverted PSC and flexible device applications. In addition, further investigations into degradation mechanisms are needed. For example, UV light degradation mechanisms at the TiO_2/perovskite interface are highly characterized by speculation and lack empirical evidence. Further knowledge of the origins of the degradation of the PSC may open the door to new and more effective stabilization techniques. The degradation methods studied so far also focus on one perovskite absorber, leading to questions about how degradation methods might change if atoms in the perovskite lattice are interchanged. For example, since UV light stability appears to be heavily dependent on the negativity of the halogen, perhaps studies on UV light stability are warranted on other perovskites where the iodine atom in $MAPbI_3$ is exchanged.

Many PSC stability studies focus on how the cell interacts with environmental conditions following production. However, little is known about the potential effects of variations in the manufacturing process on the stability of the PSC. For example, oxygen levels during fabrication can change the hole mobility of spiro-OMeTAD, and fabrication temperatures can affect the concentration of defects already present in the perovskite absorber before degradation even occurs. A closer look at the details of the manufacturing process will certainly shed light on the processes that maximize the stability of the PSC.

 This journal is © The Royal Society of Chemistry 2021

Published on 26 2021. Downloaded on 17.07.24 21:29:47.

Conflicts of interest

There are no conflicts to declare.

Acknowledgements

The first draft of this manuscript was written by Dennis (Mac) Jones, and was finalized by his colleagues at the Energy Materials Laboratories at the Georgia Institute of Technology, who are proud of Mac's achievements and celebrate him and his manuscript. We thank the Georgia Institute of Technology for the financial support.

References

1 Best Research-Cell Efficiency Chart|Photovoltaic Research|NREL, https://www.nrel.gov/pv/cell-efficiency.html, (accessed 28 July 2021).
2 Y. Ju, S. Y. Park, K. M. Yeom, J. H. Noh and H. S. Jung, *ACS Appl. Mater. Interfaces*, 2019, **11**, 11537–11544.
3 Y. Chen, L. Zhang, Y. Zhang, H. Gao and H. Yan, *RSC Adv.*, 2018, **8**, 10489–10508.
4 M. Liu, M. B. Johnston and H. J. Snaith, *Nature*, 2013, **501**, 395–398.
5 A. Jaffe, Y. Lin, C. M. Beavers, J. Voss, W. L. Mao and H. I. Karunadasa, *ACS Cent. Sci.*, 2016, **2**, 201–209.
6 J. P. Bastos, G. Uytterhoeven, W. Qiu, U. W. Paetzold, D. Cheyns, S. Surana, J. Rivas, M. Jaysankar, W. Song, T. Aernouts, J. Poortmans and R. Gehlhaar, *ACS Appl. Mater. Interfaces*, 2019, **11**, 16517–16526.
7 G. Niu, W. Li, F. Meng, L. Wang, H. Dong and Y. Qiu, *J. Mater. Chem. A*, 2014, **2**, 705–710.
8 F. Bella, G. Griffini, J. P. Correa-Baena, G. Saracco, M. Grätzel, A. Hagfeldt, S. Turri and C. Gerbaldi, *Science*, 2016, **354**, 203–206.
9 Y. J. Yoon, Y. Chang, S. Zhang, M. Zhang, S. Pan, Y. He, C. H. Lin, S. Yu, Y. Chen, Z. Wang, Y. Ding, J. Jung, N. Thadhani, V. V. Tsukruk, Z. Kang and Z. Lin, *Adv. Mater.*, 2019, **31**, 1901602.
10 Y. Han, S. Meyer, Y. Dkhissi, K. Weber, J. M. Pringle, U. Bach, L. Spiccia and Y. B. Cheng, *J. Mater. Chem. A*, 2015, **3**, 8139–8147.
11 Y. Il Lee, N. J. Jeon, B. J. Kim, H. Shim, T. Y. Yang, S. Il Seok, J. Seo and S. G. Im, *Adv. Energy Mater.*, 2018, **8**, 1701928.
12 F. Matteocci, L. Cinà, E. Lamanna, S. Cacovich, G. Divitini, P. A. Midgley, C. Ducati and A. Di Carlo, *Nano Energy*, 2016, **30**, 162–172.
13 J. Idígoras, F. J. Aparicio, L. Contreras-Bernal, S. Ramos-Terrón, M. Alcaire, J. R. Sánchez-Valencia, A. Borras, Á. Barranco and J. A. Anta, *ACS Appl. Mater. Interfaces*, 2018, **10**, 11587–11594.
14 L. Shi, T. L. Young, J. Kim, Y. Sheng, L. Wang, Y. Chen, Z. Feng, M. J. Keevers, X. Hao, P. J. Verlinden, M. A. Green and A. W. Y. Ho-Baillie, *ACS Appl. Mater. Interfaces*, 2017, **9**, 25073–25081.
15 V. H. Dalvi and P. J. Rossky, *Proc. Natl. Acad. Sci. U. S. A.*, 2010, **107**, 13603–13607.
16 G. Griffini, F. Bella, F. Nisic, C. Dragonetti, D. Roberto, M. Levi, R. Bongiovanni and S. Turri, *Adv. Energy Mater.*, 2015, **5**, 1401312.
17 H. Liu, M. Wang, J. Bian, Y. Feng, Z. Wang, B. Zhang and Y. Shi, *Appl. Phys. Lett.*, 2018, **113**, 23902.
18 C. Wu, K. Wang, X. Feng, Y. Jiang, D. Yang, Y. Hou, Y. Yan, M. Sanghadasa and S. Priya, *Nano Lett.*, 2019, **19**, 1251–1259.
19 L. Tian, Z. Hu, X. Liu, Z. Liu, P. Guo, B. Xu, Q. Xue, H. L. Yip, F. Huang and Y. Cao, *ACS Appl. Mater. Interfaces*, 2019, **11**, 5289–5297.
20 J. Yang, C. Liu, C. Cai, X. Hu, Z. Huang, X. Duan, X. Meng, Z. Yuan, L. Tan and Y. Chen, *Adv. Energy Mater.*, 2019, **9**, 1900198.
21 X. Li, M. Ibrahim Dar, C. Yi, J. Luo, M. Tschumi, S. M. Zakeeruddin, M. K. Nazeeruddin, H. Han and M. Grätzel, *Nat. Chem.*, 2015, **7**, 703–711.
22 T. H. Han, J. W. Lee, C. Choi, S. Tan, C. Lee, Y. Zhao, Z. Dai, N. De Marco, S. J. Lee, S. H. Bae, Y. Yuan, H. M. Lee, Y. Huang and Y. Yang, *Nat. Commun.*, 2019, **10**, 1–10.
23 K. Yao, X. Wang, Y. X. Xu, F. Li and L. Zhou, *Chem. Mater.*, 2016, **28**, 3131–3138.
24 J. Wei, F. Huang, S. Wang, L. Zhou, P. Jin, Y. Xin, Z. Cai, Z. Yin, Q. Pang and J. Z. Zhang, *ChemNanoMat*, 2018, **4**, 649–655.
25 D. J. Fairfield, H. Sai, A. Narayanan, J. V. Passarelli, M. Chen, J. Palasz, L. C. Palmer, M. R. Wasielewski and S. I. Stupp, *J. Mater. Chem. A*, 2019, **7**, 1687–1699.
26 C. Carrillo-Carrión, P. del Pino and B. Pelaz, *Appl. Mater. Today*, 2019, **15**, 562–569.
27 X. Shan, S. Zhang, M. Zhou, T. Geske, M. Davis, A. Hao, H. Wang and Z. Yu, *Adv. Mater. Interfaces*, 2019, **6**, 1801686.
28 G. W. Kim, G. Kang, J. Kim, G. Y. Lee, H. Il Kim, L. Pyeon, J. Lee and T. Park, *Energy Environ. Sci.*, 2016, **9**, 2326–2333.
29 J. Qiu, Y. Qiu, K. Yan, M. Zhong, C. Mu, H. Yan and S. Yang, *Nanoscale*, 2013, **5**, 3245–3248.
30 Y. S. Kwon, J. Lim, H. J. Yun, Y. H. Kim and T. Park, *Energy and Environmental Science*, Royal Society of Chemistry, 2014, vol. 7, pp. 1454–1460.
31 E. H. Jung, N. J. Jeon, E. Y. Park, C. S. Moon, T. J. Shin, T. Y. Yang, J. H. Noh and J. Seo, *Nature*, 2019, **567**, 511–515.
32 F. Di Giacomo, S. Razza, F. Matteocci, A. D'Epifanio, S. Licoccia, T. M. Brown and A. Di Carlo, *J. Power Sources*, 2014, **251**, 152–156.
33 M. Cai, V. T. Tiong, T. Hreid, J. Bell and H. Wang, *J. Mater. Chem. A*, 2015, **3**, 2784–2793.
34 D. Zou, F. Yang, Q. Zhuang, M. Zhu, Y. Chen, G. You, Z. Lin, H. Zhen and Q. Ling, *ChemSusChem*, 2019, **12**, 1155–1161.
35 K. Wang, H. Chen, T. Niu, S. Wang, X. Guo and H. Wang, *Nanomaterials*, 2019, **9**, 935.
36 Y. Bai, Q. Dong, Y. Shao, Y. Deng, Q. Wang, L. Shen, D. Wang, W. Wei and J. Huang, *Nat. Commun.*, 2016, **7**, 1–9.
37 C. Wu, K. Wang, Y. Yan, D. Yang, Y. Jiang, B. Chi, J. Liu, A. R. Esker, J. Rowe, A. J. Morris, M. Sanghadasa and S. Priya, *Adv. Funct. Mater.*, 2019, **29**, 1804419.

Published on 26 2021. Downloaded on 17.07.24 21:29:47.

38 C. Quarti, E. Mosconi, J. M. Ball, V. D'Innocenzo, C. Tao, S. Pathak, H. J. Snaith, A. Petrozza and F. De Angelis, *Energy Environ. Sci.*, 2016, **9**, 155–163.
39 B. P. P. Dhamaniya, P. Chhillar, B. Roose, V. Dutta and S. K. Pathak, *ACS Appl. Mater. Interfaces*, 2019, **11**, 22228–22239.
40 Z. Li, M. Yang, J. S. Park, S. H. Wei, J. J. Berry and K. Zhu, *Chem. Mater.*, 2016, **28**, 284–292.
41 A. Amat, E. Mosconi, E. Ronca, C. Quarti, P. Umari, M. K. Nazeeruddin, M. Grätzel and F. De Angelis, *Nano Lett.*, 2014, **14**, 3608–3616.
42 W. Travis, E. N. K. Glover, H. Bronstein, D. O. Scanlon and R. G. Palgrave, *Chem. Sci.*, 2016, **7**, 4548–4556.
43 S. N. Habisreutinger, T. Leijtens, G. E. Eperon, S. D. Stranks, R. J. Nicholas and H. J. Snaith, *Nano Lett.*, 2014, **14**, 5561–5568.
44 T. Matsui, I. Petrikyte, T. Malinauskas, K. Domanski, M. Daskeviciene, M. Steponaitis, P. Gratia, W. Tress, J. P. Correa-Baena, A. Abate, A. Hagfeldt, M. Grätzel, M. K. Nazeeruddin, V. Getautis and M. Saliba, *ChemSusChem*, 2016, **9**, 2567–2571.
45 J. Xu, O. Voznyy, R. Comin, X. Gong, G. Walters, M. Liu, P. Kanjanaboos, X. Lan and E. H. Sargent, *Adv. Mater.*, 2016, **28**, 2807–2815.
46 M. Petrović, T. Maksudov, A. Panagiotopoulos, E. Serpetzoglou, I. Konidakis, M. M. Stylianakis, E. Stratakis and E. Kymakis, *Nanoscale Adv.*, 2019, **1**, 3107–3118.
47 P. J. S. Rana, R. K. Gunasekaran, S. H. Park, V. Tamilavan, S. Karuppanan, H. J. Kim and K. Prabakar, *J. Phys. Chem. C*, 2019, **123**, 8560–8568.
48 X. Lv, G. Xiao, X. Feng, J. Cao, X. Yao and J. Liu, *Dyes Pigm.*, 2019, **160**, 957–961.
49 H. Hwang, S. Park, J. H. Heo, W. Kim, H. Ahn, T. S. Kim, S. H. Im and H. J. Son, *J. Power Sources*, 2019, **418**, 167–175.
50 S. Ito, S. Tanaka, K. Manabe and H. Nishino, *J. Phys. Chem. C*, 2014, **118**, 16995–17000.
51 H. Sohrabpoor, G. Puccetti and N. E. Gorji, *RSC Adv.*, 2016, **6**, 49328–49334.
52 W. Li, W. Zhang, S. Van Reenen, R. J. Sutton, J. Fan, A. A. Haghighirad, M. B. Johnston, L. Wang and H. J. Snaith, *Energy Environ. Sci.*, 2016, **9**, 490–498.
53 A. M. Nardes, M. Kemerink, M. M. de Kok, E. Vinken, K. Maturova and R. A. J. Janssen, *Org. Electron.*, 2008, **9**, 727–734.
54 C. H. Tsai, N. Li, C. C. Lee, H. C. Wu, Z. Zhu, L. Wang, W. C. Chen, H. Yan and C. C. Chueh, *J. Mater. Chem. A*, 2018, **6**, 12999–13004.
55 T. Y. Yang, N. J. Jeon, H. W. Shin, S. S. Shin, Y. Y. Kim and J. Seo, *Adv. Sci.*, 2019, **6**, 1900528.
56 K. Mahesh, S. Karpagam, T. Putnin, H. Le, T. T. Bui, K. Ounnunkad and F. Goubard, *J. Photochem. Photobiol., A*, 2019, **371**, 238–247.
57 D. Yang, X. Zhang, K. Wang, C. Wu, R. Yang, Y. Hou, Y. Jiang, S. Liu and S. Priya, *Nano Lett.*, 2019, **19**, 3313–3320.
58 C. Liu, J. Tu, X. Hu, Z. Huang, X. Meng, J. Yang, X. Duan, L. Tan, Z. Li and Y. Chen, *Adv. Funct. Mater.*, 2019, **29**, 1808059.
59 L. Hu, M. Li, K. Yang, Z. Xiong, B. Yang, M. Wang, X. Tang, Z. Zang, X. Liu, B. Li, Z. Xiao, S. Lu, H. Gong, J. Ouyang and K. Sun, *J. Mater. Chem. A*, 2018, **6**, 16583–16589.
60 X. Sun, X. Yu and Z. Li, *ACS Appl. Energy Mater.*, 2020, **3**, 10282–10302.
61 X. Sun, Z. Li, X. Yu, X. Wu, C. Zhong, D. Liu, D. Lei, A. K.-Y. Jen, Z. Li and Z. Zhu, *Angew. Chem.*, 2021, **133**, 7303–7309.
62 Q. Xiao, J. Tian, Q. Xue, J. Wang, B. Xiong, M. Han, Z. Li, Z. Zhu, H. L. Yip and Z. Li, *Angew. Chem., Int. Ed.*, 2019, **58**, 17724–17730.

This journal is © The Royal Society of Chemistry 2021